



## Article

# Evaluation of SST Data Products from Multi-Source Satellite Infrared Sensors in the Bohai-Yellow-East China Sea

Changlong Feng<sup>1</sup>, Wenbin Yin<sup>1,\*</sup> , Shuangyan He<sup>2,3,4</sup>, Mingjun He<sup>2,3</sup> and Xiaoxia Li<sup>5</sup>

<sup>1</sup> College of Marine Science and Technology, Zhejiang Ocean University, Zhoushan 316022, China; s20070700022@zjou.edu.cn

<sup>2</sup> Ocean College, Zhejiang University, Zhoushan 316021, China; hesy@zju.edu.cn (S.H.); 12134023@zju.edu.cn (M.H.)

<sup>3</sup> Hainan Institute, Zhejiang University, Sanya 572025, China

<sup>4</sup> State Key Laboratory of Satellite Ocean Environment Dynamics, Second Institute of Oceanography, Ministry of Natural Resources, Hangzhou 310012, China

<sup>5</sup> Meteorological Observation Center of China Meteorological Administration, Beijing 100081, China; lxxaoc@cma.gov.cn

\* Correspondence: yinwenbin@zjou.edu.cn

**Abstract:** The measurement of sea surface temperature (SST) is of utmost importance in the realm of oceanography. The increasing utilization of satellite data in SST research has highlighted the crucial need to compare and evaluate various satellite data sources. Using iQuam2 in situ SST data, this study aims to assess the accuracy of SST datasets obtained from three polar-orbiting satellites (AVHRR, Modis-Aqua, and Modis-Terra) and one geostationary satellite (Himawari-8) in the Bohai-Yellow-East China Sea (BYECS) throughout 2019. The results showed a strong correlation between satellite and in situ data, with R correlation coefficients exceeding 0.99. However, the accuracy of the satellite datasets exhibited some variability, with Himawari-8 showing the highest deviation error and MODIS-Aqua showing the least. Subsequently, the Modis-Aqua data were used as a benchmark to evaluate the SST data of the other three satellites over the previous six years (July 2015–June 2021). The results indicate that, in addition to intricate temporal variations, the deviations of the three satellites from Modis-Aqua also show significant spatial disparities due to the effect of seawater temperature. Compared to Modis-Aqua, the deviation of Himawari-8 generally displayed a negative trend in BYECS and showed pronounced seasonal variation. The deviation of AVHRR showed a negative trend across all regions except for a substantial positive value in the coastal region, with the time variation exhibiting intricate features. The SST values obtained from MODIS-Terra exhibited only marginal disparities from MODIS-Aqua, with positive values during the day and negative values at night. All three satellites showed significantly abnormal bias values after December 2020, indicating that the MODIS-Aqua-derived SST reference dataset may contain outliers beyond this period. In conclusion, the accuracy of the four satellite datasets varies across different regions and time periods. However, they could be effectively utilized and integrated with relevant fusion algorithms to synthesize high-precision datasets in the future.

**Keywords:** sea surface temperature; Bohai-Yellow-East China Sea; iQuam2; Himawari-8; AVHRR; MODIS; comparison and evaluation



**Citation:** Feng, C.; Yin, W.; He, S.; He, M.; Li, X. Evaluation of SST Data Products from Multi-Source Satellite Infrared Sensors in the Bohai-Yellow-East China Sea. *Remote Sens.* **2023**, *15*, 2493. <https://doi.org/10.3390/rs15102493>

Academic Editor: Feng Ling

Received: 14 March 2023

Revised: 2 May 2023

Accepted: 7 May 2023

Published: 9 May 2023



**Copyright:** © 2023 by the authors. Licensee MDPI, Basel, Switzerland. This article is an open access article distributed under the terms and conditions of the Creative Commons Attribution (CC BY) license (<https://creativecommons.org/licenses/by/4.0/>).

## 1. Introduction

The sea surface temperature (SST) is a comprehensive parameter that can characterize solar radiation, air–sea interactions, and the dynamic processes within the ocean interior. It can help us understand, monitor, and forecast ocean parameters of air–sea interaction and provide important information on the global climate system [1]. Not only does it play a significant role in the study of water vapor and heat exchange at the sea surface, it

also serves as a crucial indicator for the investigation of ocean circulation, fronts, water masses, and other dynamic processes occurring within the ocean [2]. SST plays a key role in controlling the Earth's climate system on a global scale, which underlines the importance of having accurate measurements of SST and monitoring of SST at different times and spaces [3,4]. Multi-scale variation of SST has become a focal point in oceanographic research, as it aids in the study of the relationship between global warming and oceanic heat content. Additionally, it provides insight into the impact of global climate anomalies on both oceanic and atmospheric dynamic processes [5,6].

SST data are primarily obtained through shipborne or buoy in situ observations and satellite remote sensing. The in situ data have reliable accuracy, but their spatial resolution and coverage are relatively low. Additionally, the quality and completeness of the in situ data are not optimal because the matched database contains a small number of outliers [7]. As satellite SST data can be acquired with high spatio-temporal resolution and large area quasi-synchronization, they are increasingly used in various studies of oceanography. Satellite SST data from infrared sensors have better spatial resolution, i.e., around 1–4 km, compared to microwave radiometer data, with resolution of around 25 km [8,9], and are widely used at present to show SST spatial distribution and temporal variation. Satellite infrared data are easily affected by cloud cover, resulting in less effective observation data. Especially in coastal areas, cloud cover can cause gaps in satellite data [10]. Therefore, multi-source satellite data are also fused to improve the spatial coverage of SST products. Several infrared SST datasets are available now and have been used in various oceanographic studies. However, different SST datasets are processed with different accuracy from different sensors and inversion algorithms. Therefore, it is important and necessary to perform accuracy verification and cross-comparisons on multi-source satellite data.

Gong et al. [11] validated the accuracy of MODIS-Terra SST daytime and nighttime products by comparing them with the timing SST measurements from ships in the East China Sea (ECS) in February, May, August, and November of 2001. They found that the MODIS SST daily products demonstrated good accuracy with a mean absolute percentage error (MAPE) of below 5%. Similarly, Hao et al. [12] used in situ buoy data to examine and validate the MODIS Aqua and Terra SST products for coastal waters in the Yellow Sea. They discovered that the MODIS SST agreed well with in situ buoy SST, with squared correlation coefficients  $R^2$  of 0.989 for Terra and 0.987 for Aqua. Saleh et al. [13] employed the iQuam SST dataset to validate MODIS SSTs in the Arabian Gulf and concluded that MODIS SSTs had a slight cool nighttime bias compared to iQuam SSTs, with a mean  $\pm$  SD of  $-0.36 \pm 0.77$  °C for Aqua and  $-0.27 \pm 0.83$  °C for Terra from July 2002 to May 2020. The daytime MODIS SST observations displayed a lower negative bias for both Aqua (Bias =  $-0.052$  °C, SD = 0.93 °C) and Terra (Bias =  $-0.24$  °C, SD = 0.90 °C). After comparing MODIS SST data with observations from an oceanographic buoy in the SE Baltic and two coastal hydrographic stations in the Curonian Lagoon, Igor et al. [14] found that the daytime SST from MODIS exhibited excellent agreement with in situ data, with a positive bias (RMSD) not exceeding 0.49 °C (1.31 °C) and  $R^2$  not lower than 0.78. Shuva, M.S.H. et al. [15] used MODIS-T to compare day and night SST in the northern Bay of Bengal; the results showed that MODIS-T exhibited a significant moderate correlation ( $r = 0.54$ ) with NODC in situ data.

Chen et al. [16] conducted a comparison between AVHRR SST products and buoy SSTs in the stable operational period of each satellite in the Northwest Pacific Ocean. Their findings revealed that the SST product accuracy varied for each satellite during different periods. In the northern South China Sea (NSCS), the accuracy of AVHRR and TMI daytime and nighttime SSTs were validated using in situ SSTs from drifting buoys and well-calibrated sensors on R/V Shiyan 3. The results showed that the AVHRR SSTs had regional biases of approximately  $-0.4$  °C against drifting buoy SSTs [17]. Another study by Xi et al. [18] assessed the accuracy of AVHRR, MODIS-Aqua, and MODIS-Terra using Argo data for the Northwest Pacific region between 2003–2009. The findings revealed that there

was a bias of  $\pm 0.2$  °C between infrared products and Argo products, with an RMSE within 0.8 °C and significant seasonal and diurnal cycles.

Leveraging the Advanced Himawari Imager's (AHI) data onboard the state-of-the-art geostationary meteorological satellite Himawari-8, the Japan Aerospace Exploration Agency (JAXA) collaborated with the Japan Meteorological Agency (JMA) to unveil a new SST product in 2016. This novel product boasts observation frequencies every 10 min and an impressive spatial resolution of 2 km. In contrast to the SST products of polar-orbiting satellites, this new product offers superior temporal resolution and wider spatial coverage, making it ideal for investigating short-term dynamic oceanic processes. Several scholars have used Himawari-8 data to study and analyze many ocean dynamics elements such as upwelling [19], currents [20], fronts [21], Chl-a [22], marine heatwaves [23], and so on, indicating that this high-resolution dataset is being widely used.

The meticulous evaluation conducted by JAXA, which compared Himawari-8 SST with drifting and tropical moored buoy data, demonstrated a root-mean-square difference of approximately 0.59 K and a bias of approximately  $-0.16$  K. Moreover, a few studies have also attested to the accuracy of Himawari-8 SST. Angela et al. [24] compared the SST of Japanese geostationary satellite MTSAT-2 and Himawari-8 with the subsurface in situ temperature measurements from the Tropical Atmosphere Ocean (TAO) array and self-recording thermometers at the depths of corals in the Great Barrier Reef. The results indicated that the Himawari-8 provides more accurate SST measurements compared to those from MTSAT-2. At various locations where in situ measurements were taken, the mean Himawari-8 SST error showed an improvement of about 0.15 K. In another study, Tu et al. [25] validated the Himawari-8 full-disk SST using iQuam2 in situ SST and found small biases, i.e., between  $-0.11$  and  $-0.03$  K, with a root mean square error (RMSE) of between 0.58 and 0.73 K.

In summary, while several studies have validated and cross-compared satellite infrared sea surface temperature (SST) data using different field data in various oceanic water areas, a comprehensive evaluation of commonly used SST datasets is still necessary. The differing accuracy of SST data employed by researchers can render it challenging to determine the reliability and comparability of their findings. In this paper, we evaluate the accuracy of four satellites that remote sense infrared sea surface temperature data (namely, Himawari-8, AVHRR, Modis-T, and Modis-A) in the Bohai-Yellow-East China Sea (BYECS) using iQuam2 SST in situ data from 2020. We compare the other three satellite datasets with that of MODIS-Aqua as the validation dataset and analyze the spatial and temporal distributions of sea surface temperature products, as well as the differences among the four satellite datasets, during both daytime and nighttime, to evaluate the characteristics of the four datasets. The proposed step-by-step research is illustrated in the following block diagram (Figure 1).

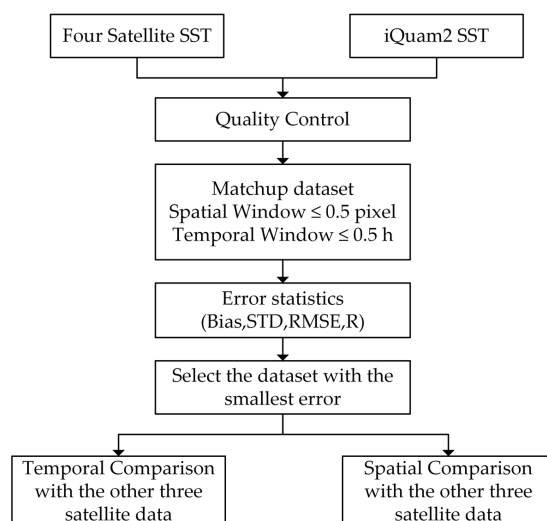


**Figure 1.** Flow diagram of the research methods.

## 2. Materials and Methods

### 2.1. Study Area

The BYECS, encompassing the Bohai Sea, Yellow Sea, and East China Sea, is situated at 117–130° E and 24–40° N and is an important confluence point of China coastal water masses, shelf mixed water masses, and Kuroshio water masses (refer to Figure 2). Additionally, it is characterized by strong tidal systems and significant river inflows, making its hydrological environment exceedingly intricate. This area has been a topic of interest for oceanographers for a long time, as variations in the marine environment have a direct impact on China's inland climate and the utilization of coastal marine resources. Given its shallow water depth and limited volume capacity, coupled with the effects of local complex dynamic processes and external variation signals, the hydrological elements in the BYECS exhibit multi-scale spatiotemporal variation characteristics, rendering it a crucial and distinct research region.

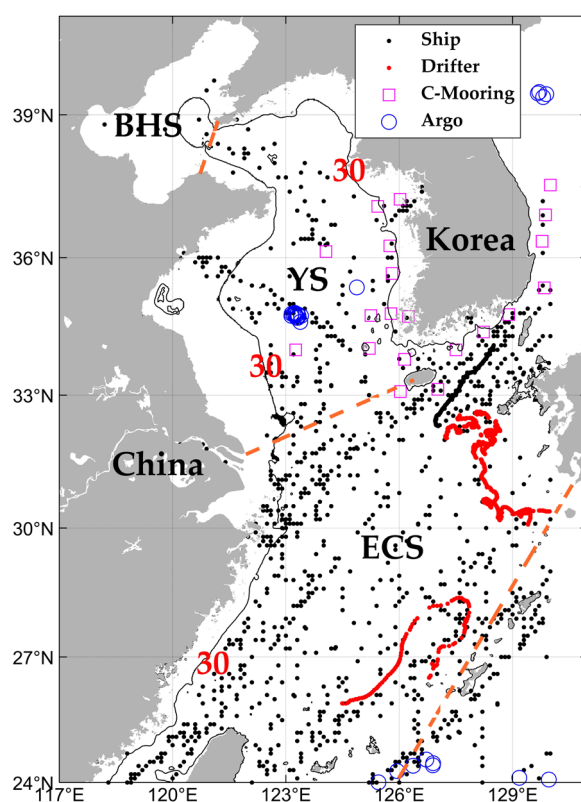


**Figure 2.** Map of the Bohai–Yellow–East China Sea Region. Points in the figure are the distribution of iQuam2 SST data points in January 2020. The orange dotted lines are the boundaries of the three seas. **BHS:** Bohai Sea; **YS:** Yellow Sea; **ECS:** East China Sea. The black line is the isobath of 30 m.

### 2.2. Dataset

#### 2.2.1. Himawari-8 SST

The Himawari-8 satellite, which serves as a geostationary meteorological apparatus, was developed by the Japan Meteorological Agency to supplant the former Japanese Multifunctional Transport Satellite 2 (MTSAT-2) and was operationalized on the 7 July 2015. Positioned at 140.7°E, it captures images of the Earth between 80°E to 160°W and at latitudes ranging from 60°N to 60°S. Onboard the Himawari-8 is the Advanced Himawari Imager (AHI), an optical radiometer. AHI has a scanning frequency of 10 min for the full disk and 2.5 min for the regions adjacent to Japan. The SSTs are obtained using a novel quasi-physical SST algorithm which estimates skin SSTs by solving a parameterized IR radiative transfer equation and utilizing the 8.6  $\mu\text{m}$ , 10.4  $\mu\text{m}$ , and 11.8  $\mu\text{m}$  infrared bands to solve the inverse of the parametric infrared radiative transfer equation [26]. The spatial

resolution of this dataset is 2 km, and its temporal resolution is 10 min. Hourly and monthly Himawari-8 SST data spanning six years (July 2015–June 2021) were employed in this study (Figure 3a). The dataset comes in different quality levels, and only data with quality levels greater than 4 were selected for the present research. This dataset is downloadable from the website <https://www.eorc.jaxa.jp/ptree/> (accessed on 12 June 2022).

#### 2.2.2. AVHRR SST

The AVHRR Pathfinder version 5.3 (PFV5.3) L3C SST dataset (Figure 3b) is a comprehensive and enduring climate data record, spanning from 1981 to the present day. This dataset draws upon the historical lineage of the Pathfinder SST [27]. The dataset encompasses global, twice-daily (Day and Night) 4 km SST derived from measurements obtained by Advanced-Very-High-Resolution-Radiometer (AVHRR) instruments that are affixed to the NOAA polar-orbiting satellites. This SST product is calculated using a regression-based non-linear algorithm that is founded on a contemporary system based on the NASA SeaWiFS Data Analysis System SeaDAS (version 6.4). The algorithm has been applied consistently across the complete timeline of the product (August 1981–Present) [28,29]. In this study, the along-track SST was employed to compare with in situ data for verification, and six years (July 2015–June 2021) of daily SST data were amalgamated into monthly SST data. This dataset has been categorized from 0 (low) to 7 (high) according to quality. Only data with quality flags greater than or equal to 5 have been chosen in this analysis. This dataset can be downloaded from the website (<https://www.ncei.noaa.gov/products/avhrr-pathfinder-sst/>, accessed on 21 June 2022).

#### 2.2.3. MODIS SST

The Moderate Resolution Imaging Spectroradiometer (MODIS) is a crucial instrument aboard both the Terra (Figure 3c) and Aqua (Figure 3d) satellites, which have distinct orbits around the Earth. Terra's trajectory passes from north to south across the equator in the morning, while Aqua passes from south to north over the equator in the afternoon. These satellites can capture data in 36 spectral bands, allowing them to view the entire surface of the Earth every 1 to 2 days [30]. The MODIS Sea Surface Temperature (SST) product consists of one thermal-IR SST parameter and one mid-IR SST parameter, but the mid-IR bands close to 4  $\mu\text{m}$  are influenced by intense reflective sources, such as sun glint, rendering the mid-IR SST product inappropriate for daytime use. Therefore, we only validated the thermal-IR SST using non-linear SST (NLSST) algorithms in this study. The level 2 data were used to compare with in situ data to validate the accuracy, while the six years of Level 3 data from July 2015 to June 2021 were utilized for comparison with other satellite data products. This dataset can be obtained from the website (<https://oceandata.sci.gsfc.nasa.gov/directdataaccess/>, accessed on 6 June 2022).

#### 2.2.4. iQuam2 SST

In situ sea surface temperature (SST) measurements are often regarded as the most reliable reference to validate the SST obtained from satellite observations. In this manuscript, the in situ SST measurements were sourced from the second version of the in situ SST Quality Monitor (iQuam2). The iQuam2 system was developed at the NOAA Center for Satellite Application and Research (STAR) and has three primary functions [31]: (1) quality control (QC) of in situ SSTs; (2) online monitoring of QCed in situ SSTs; and (3) provision of reformatted in situ SST data with appended quality level and flags. This dataset comprises a variety of data sources, including commercial ships, drifting buoys, tropical moored buoys, coastal moored buoys, Argo floats data, and drifter SST data, among others. Xu et al. [32] calculated the standard deviations (STD) for each type of iQuam2 data using triple-collocation analyses. The results show that the STD of errors in iQuam2 in situ are 0.75 K for ships, 0.21–0.22 K for drifters and Argo floats, and 0.17 K and 0.40 K for tropical and coastal moorings, respectively. The assessed error level is therefore relatively low for

all types of data. The iQuam2 QC algorithm includes pre-screening, plausibility check, internal consistency check, mutual consistency check, and external consistency check steps. Besides the fundamental processing steps, the five major steps are duplicate removal (DR), platform track check (TC), SST spike check (SC), reference check (RC), and cross-platform check (XC). These steps are designed to eliminate outliers (coarse errors) while minimizing interference with the inherent statistical characteristics of the measured measurement errors. All the statistics presented on the iQuam2 webpage are based on “high accuracy” data only, i.e., quality level = 5. This measured dataset is now widely utilized [16,25,33] and can be downloaded from the website (<https://www.star.nesdis.noaa.gov/socd/sst/iquam/>, accessed on 5 June 2022).

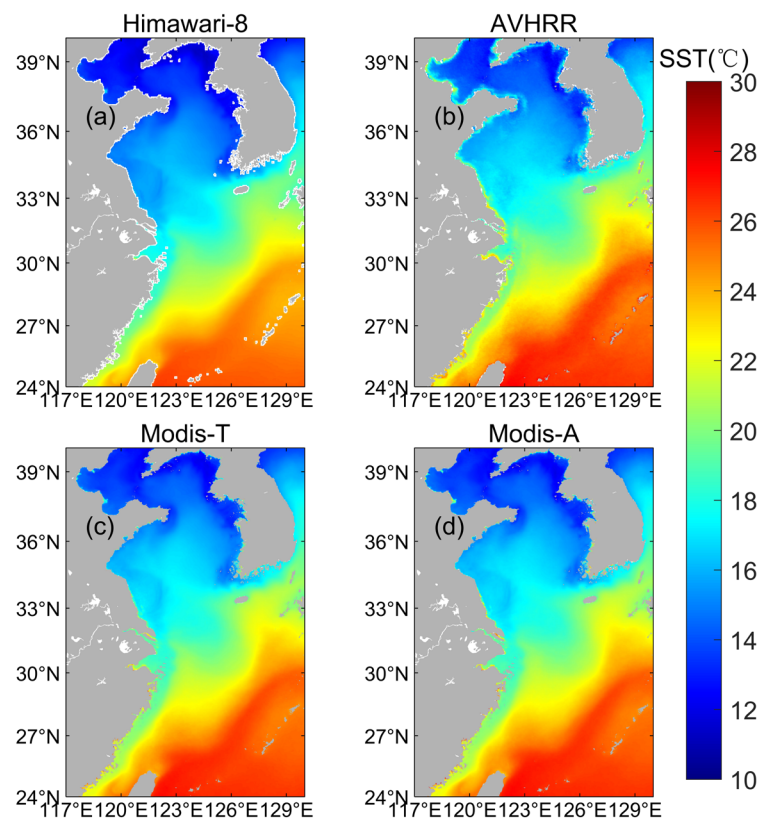


**Figure 3.** The mean SST distribution for the four satellites over a period of six years (July 2015–June 2021). The four datasets are: (a) Himawari-8; (b) AVHRR; (c) Modis-T; and (d) Modis-A.

### 2.3. Methods

#### 2.3.1. Match-Up Method

For this analysis, we utilized along-track sea surface temperature (SST) data from polar-orbiting satellites (AVHRR and MODIS), as well as hourly SST data from geostationary satellites, to perform an accuracy assessment against in situ data. Due to variations in the spatial and temporal sampling characteristics between the satellite products and in situ data, it was necessary to establish appropriate spatial ( $\Delta x$ ) and temporal ( $\Delta t$ ) windows based on the spatial resolution of the satellite products. The matching protocol employed to generate paired, collocated observations of satellite and in situ SST is outlined below:

- (1) Based on the geographic coordinates (latitude and longitude) and observation date of the in situ data, we selected the corresponding satellite products acquired on the same day as the in situ observation. Subsequently, we recorded the in situ SST value at the nearest satellite overpass time (where in situ measurements were obtained within a time window of less than 0.5 h);

$$|\Delta t| \leq 0.5 \text{ h} \quad (1)$$

- (2) The satellite SST data were selected from the  $0.5 \times 0.5$  pixel box centered on the in situ SST sample points. Each pixel represents the spatial resolution of the satellite data. Half the spatial resolution of the satellite data was used as the size of the box. To ensure the validity of the assessment results, negative SST values were excluded to avoid the impact of invalid data.

$$|\Delta x| \leq 0.5 \text{ pixel} \quad (2)$$

- (3) Next, the average effective satellite SST value within the spatial window (0.5 pixels) and the average effective in situ SST within the temporal window (0.5 h) were considered as pairs of matching data and subsequently included in the validation dataset.
- (4) In order to mitigate the impact of anomalous data, the validation dataset's standard deviation (STD) was computed, and subsequently, the matching points that exceeded  $1.5 \times \text{STD}$  were eliminated.

After completing the aforementioned procedures, we obtained a total of 33,658, 1481, 1886, and 1997 pairs of matching data for Himawari-8, AVHRR, MODIS Terra, and Aqua, respectively, throughout the year 2020. It is evident that the number of matching data pairs for geostationary satellites is significantly greater than that of polar orbit satellites, primarily due to the higher sampling frequency.

### 2.3.2. Verification and Statistics

In order to assess the accuracy and compare the differences between various satellite products, we calculated the mean deviation (Bias), standard deviation (STD), root mean square error (RMSE), and correlation coefficient (R). Bias represents the average difference between two sets of data, while STD reflects the dispersion of two sets of data relative to the average deviation; the larger the STD, the greater the degree of dispersion. RMSE reflects the degree of deviation of two sets of data and is more sensitive to outliers, making it a better indicator of the precision of the data. R reflects the degree of correlation between two sets of data. The calculation formula for each metric is as follows:

$$\text{Bias} = \frac{\sum_{i=1}^n (T_i - t_i)}{n} \quad (3)$$

$$\text{STD} = \sqrt{\frac{\sum_{i=1}^n [(T_i - t_i) - (\bar{T} - \bar{t})]^2}{n}} \quad (4)$$

$$\text{RMSE} = \sqrt{\frac{\sum_{i=1}^n (T_i - t_i)^2}{n}} \quad (5)$$

$$R = \frac{\sum_{i=1}^n (T_i - \bar{T})(t_i - \bar{t})}{\sqrt{\sum_{i=1}^n (T_i - \bar{T})^2 \times \sum_{i=1}^n (t_i - \bar{t})^2}} \quad (6)$$

where  $i$  represents the number of matching data points, while  $n$  represents the total number of matching data points.  $T$  and  $t$  denote the satellite dataset being verified and the reference dataset, respectively. The overline symbol indicates the arithmetic average.

## 3. Results

### 3.1. Results of Our Comparison with In Situ SST Data

For the purpose of verification, the annual Bias, STD, RMSE, and R of the four satellite datasets and the iQuam2 in situ data were calculated for the year 2020. The overall statistical results are presented in Figure 4 and summarized in Table 1. It can be observed that the

four satellite datasets exhibit a high degree of correlation with the in situ measured data, with R correlation coefficients above 0.99. When compared with the in situ SST data, the Biases of the four satellite-derived SST datasets were nearly  $-0.31$  °C (Himawari-8),  $-0.24$  °C (AVHRR),  $0.09$  °C (Terra), and  $0.04$  °C (Aqua), respectively. The analysis revealed that the derivation error of Himawari-8 was the highest among the four satellites, while MODIS-Aqua exhibited the lowest error. The RMSE of the four satellites also supported this conclusion. Since the spatial and temporal resolution of Himawari-8 is higher than those of the other three satellites, it is an objective fact that its sample size is much larger than those for the data of the other three satellites in the same time period. Considering that the sample size may affect the error of satellite data, we conducted a new error analysis of the data from the four satellites in 2020. In this new analysis, we selected Himawari-8 data based on the passing time of MODIS-A and discarded all data from other times. This reduced the sample size of Himawari-8 to the same order of magnitude as the other three satellites. Under the premise of ensuring that the sample sizes of the four types of satellite data would be almost the same, the results of the error analysis (not shown in this paper) showed that the error of Himawari-8 actually increased with a decrease of sample size, and the error of MODIS-A was still the lowest among the four satellites. Furthermore, compared to the in situ measured SST, the derived SST of Himawari-8 and AVHRR were underestimated, while the derived SST of the MODIS satellites were overestimated. The STD results indicate that Himawari-8 not only had a large mean error but also exhibited a significant error fluctuation, with a value of  $0.65$  °C, while MODIS-Aqua had the smallest error fluctuation.

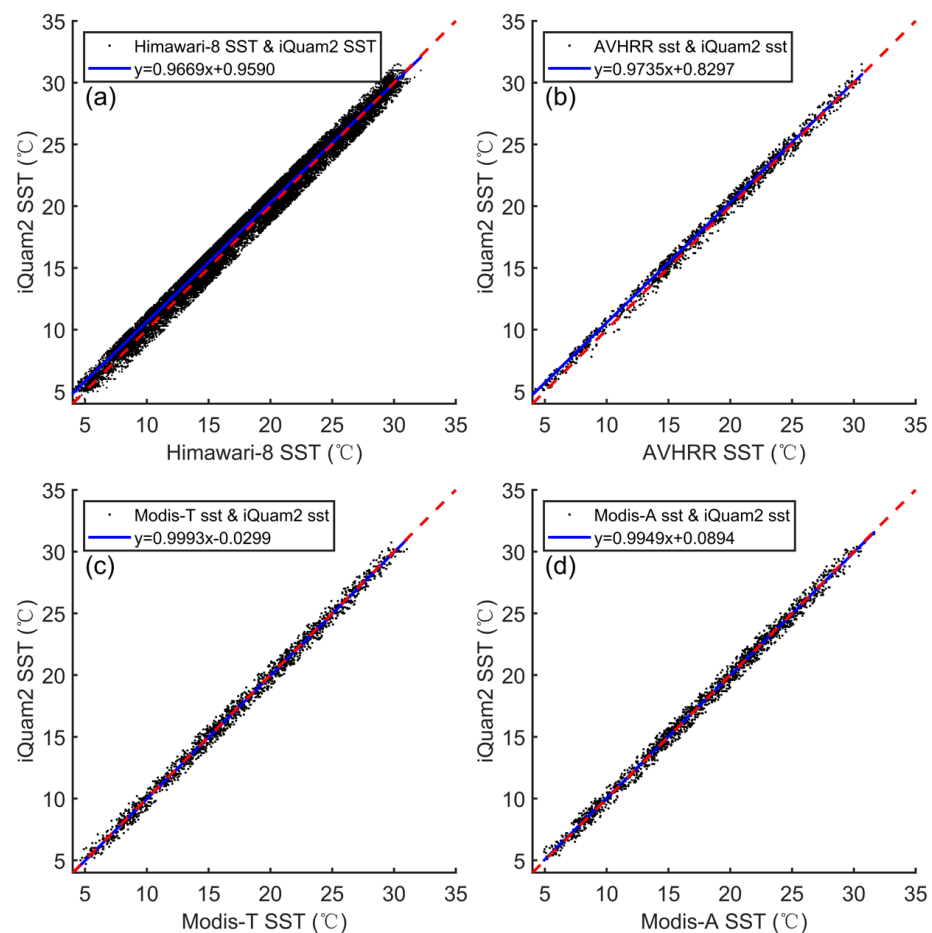


**Figure 4.** Scatter plots of Himawari-8 (a), AVHRR (b), MODIS-Terra (c), and MODIS-Aqua (d) versus iQuam2 in situ SST. The red dotted line indicates the 1:1 line.

**Table 1.** Error statistics of four satellite SST versus iQuam2 in situ SST.

SST	Num	Fitting Curve	Bias	STD	RMSE	R
Himawari-8-iQuam2	33,658	$y = 0.9669x + 0.9590$	-0.3052	0.6536	0.7214	0.9944
AVHRR-iQuam2	1481	$y = 0.9735x + 0.8297$	-0.2402	0.4537	0.5134	0.9973
Modis-T-iQuam2	1886	$y = 0.9993x - 0.0299$	0.0879	0.4485	0.4505	0.9975
Modis-A-iQuam2	1997	$y = 0.9949x + 0.0894$	0.0429	0.4431	0.4431	0.9974

Figure 5 depicts the curves of hourly error statistic parameters for the four satellites for the year 2022. While the annual errors of the four satellites were generally small, there were some collocated points with large hourly errors. Specifically, an extreme value of hourly error was observed in Himawari-8, with the maximum values of hourly Bias and RMSE (indicated by the black and blue lines, respectively) from the in situ measured data reaching up to 6 °C. The corresponding values for the other satellites did not exceed 4 °C. Additionally, the error fluctuation of Himawari-8 was also the highest, whereas the other three satellites exhibited smaller error fluctuations, with most related hourly STD (indicated by red points in Figure 5) values being less than 2 °C. Moreover, the average values of positive/negative hourly Bias (indicated by the green dotted lines in Figure 5) reveal that the errors in Himawari-8 and AVHRR SST data were higher when they were underestimated, whereas the errors in the two MODIS satellites showed the opposite trend.

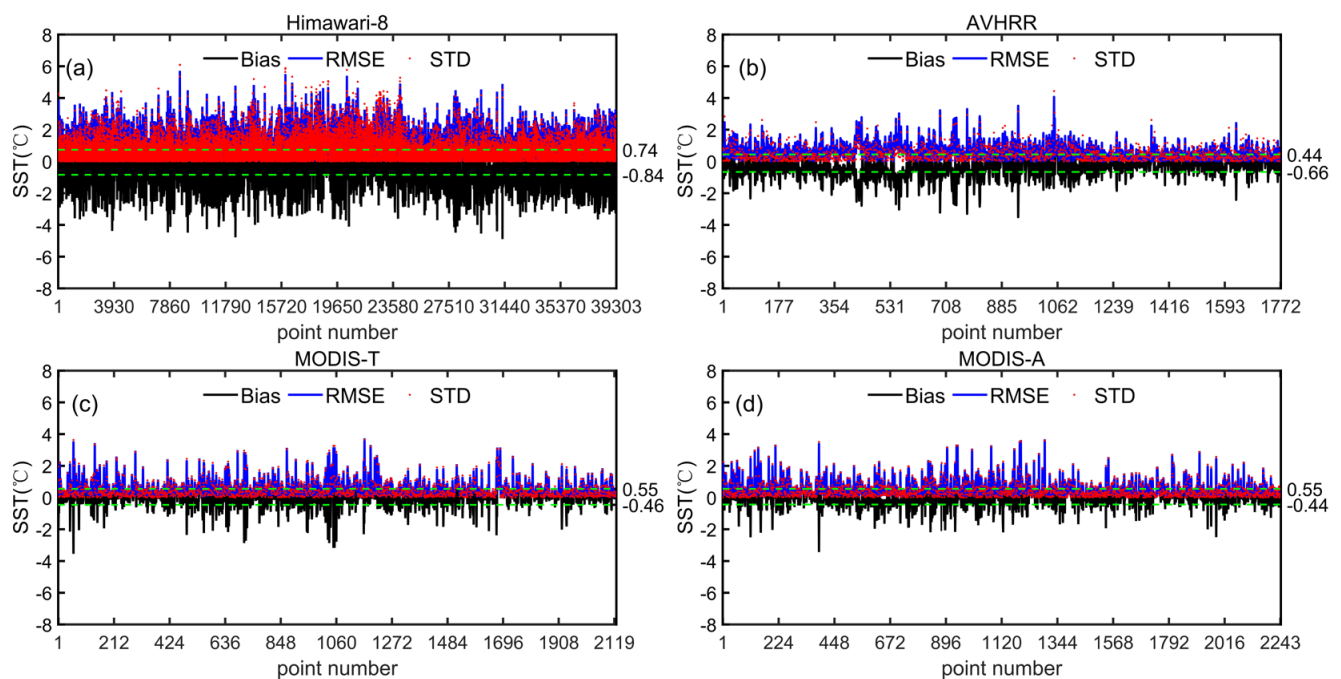


**Figure 5.** The curves of hourly error statistics for (a) Himawari-8, (b) AVHRR, (c) Modis-Terra, and (d) Modis-Aqua in the year 2020. The black/green solid line represents Bias/RMSE, respectively; the red points represent STD; the green dotted line represents the average of positive/negative bias.

### 3.2. The Cross-Comparison Results with MODIS-Aqua SST Data

In this study, the iQuam2 in situ measured SST data were utilized as the “ground truth” to validate the four satellite-retrieved SST products. However, as the major in situ data types included in the iQuam2 dataset are obtained through a combination of ships, drifters, and Argo floats, the spatial distribution of the iQuam2 dataset is non-uniform and the temporal distribution is discontinuous. To further assess the various characteristics of the satellite-derived SST products in space and time, the MODIS-Aqua SST data, which exhibited the lowest degree of error when compared to the in situ data, were employed as the validation dataset in this section. Additionally, since the resolution of the geostationary

satellite Himawari-8 SST data differs from that of the other three polar orbit satellites, it was necessary to downscale the data of Himawari-8 and interpolate them to the grid points of the polar-orbiting satellites.

Figure 6 illustrates the spatial difference of the average SST between three satellites and MODIS-Aqua over the past six years, from July 2015 to June 2021. Compared to MODIS-Aqua, the SST data obtained from Himawari-8 generally exhibited lower values in the BYECS region, with greater deviation during daytime as opposed to nighttime. Specifically, the overall sea area deviation was approximately  $-1.3\text{ }^{\circ}\text{C}$  during daytime (Figure 6a), which generally reduced to about  $-0.75\text{ }^{\circ}\text{C}$  at nighttime, except for the sea area adjacent to the Kuroshio (Figure 6d). The SST derived from AVHRR was much higher than that of MODIS-Aqua in the nearshore region (Figure 6b,e). In the sea area far from the shore, the daytime SST of AVHRR was lower than that of MODIS-Aqua, with a deviation of  $-0.18\text{ }^{\circ}\text{C}$ , while the nighttime SST was generally higher than that of MODIS-Aqua in most areas, with a deviation of  $0.27\text{ }^{\circ}\text{C}$ , particularly near the Kuroshio Current (Figure 6b,e). The SST of MODIS-Terra was only slightly different from MODIS-Aqua, exhibiting slightly lower/higher values during daytime/nighttime (Figure 6c,f).

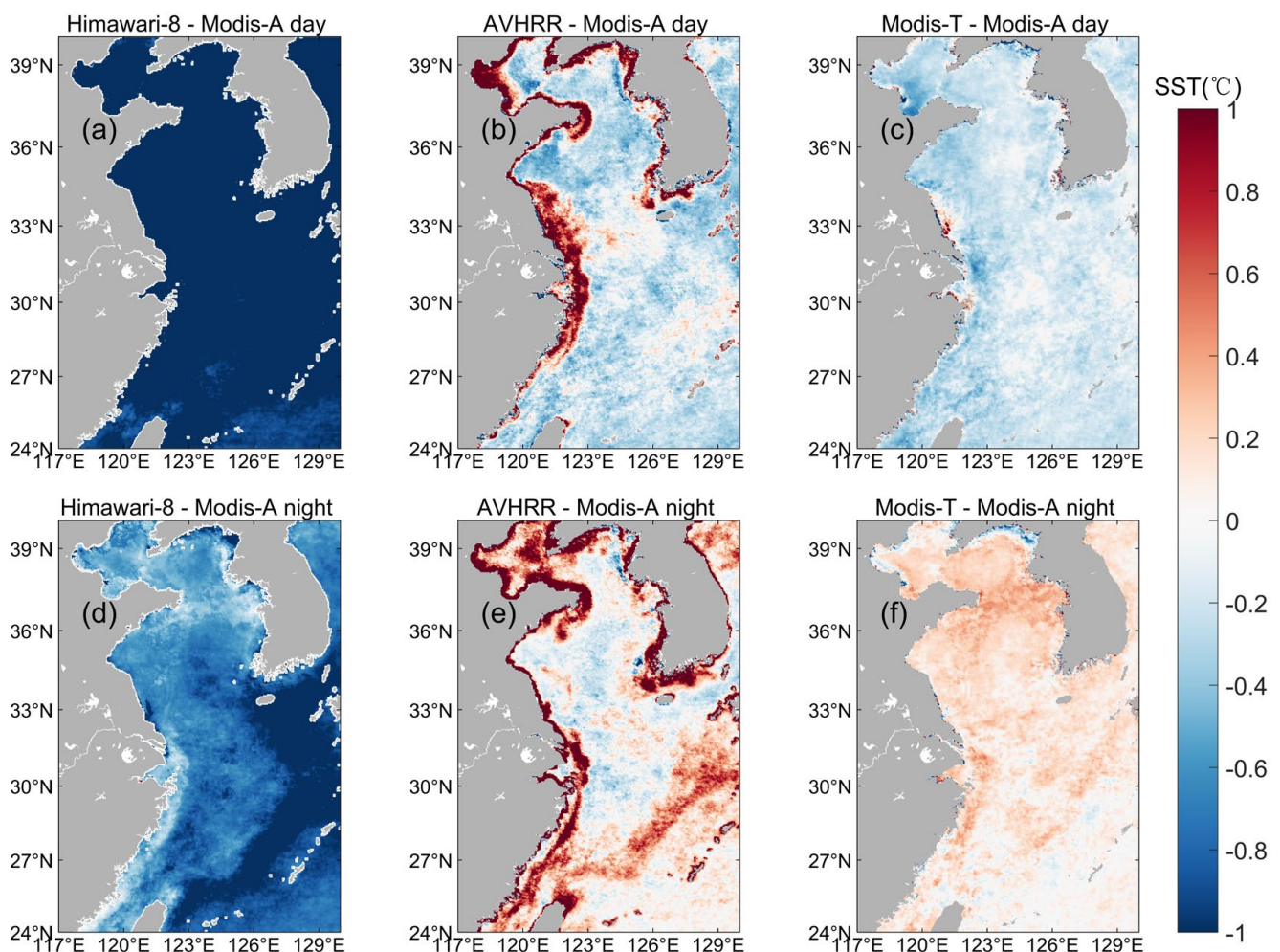


**Figure 6.** The spatial distribution of SST difference between three satellites and MODIS-Aqua. (a): Himawari-8 daytime; (b): AVHRR daytime; (c): Modis-T daytime; (d): Himawari-8 nighttime; (e): AVHRR nighttime; (f): Modis-T nighttime.

Figure 7 illustrates the distribution of SST deviation between three satellites and MODIS-Aqua at different water temperatures. The deviation of SST between Himawari-8 and MODIS-Aqua was predominantly negative and was influenced by the water temperature. The daytime SST deviation of Himawari-8 decreased with increas-

ing water temperature (Figure 7a), indicating that the retrieval error of Himawari-8 daytime SST is lower in regions with higher temperatures than in regions with lower temperatures. This conclusion is consistent with that drawn from Figure 5a, which shows that the retrieval SST error was smaller in the south of BYECS with a higher temperature than in the north of BYECS with a lower temperature. In contrast to the daytime results, the retrieval error at night increased as the water temperature increased (Figure 7d), implying that the retrieval error of nighttime SST in areas with high temperatures, such as the Kuroshio area, is larger than in other areas (Figure 6d). The deviation of AVHRR was smaller than that of Himawari-8 and increased with increasing temperature (Figure 7b,e). AVHRR exhibited different characteristics. When the error was small (i.e., the fitting curve was close to 0), the data were relatively discrete, while when the error was large, the distribution of data points was relatively concentrated (Figure 7b,e). The deviation of MODIS-Terra was the smallest and decreased with increasing water temperature (Figure 7c,f). This indicates that the error of MODIS-Terra in high-temperature areas is smaller than that in low-temperature areas (Figure 6c,f), such as the southern vs. northern areas of BYECS and the shelf sea vs. coastal sea, among others. It is also possible that the SST deviation varied with SST, because the larger dispersion values at lower SSTs caused the positive and negative SST deviation to cancel out, so that the deviation at lower SSTs was larger than the difference at higher SSTs. This feature of AVHRR was more obvious, and its deviation dispersion value was larger than the those of the other two datasets (Figure 7b,e). The results also showed a very low correlation, which was consistent with previous studies [12,34]. Although the results showed a significant change, the correlation was low, indicating the presence of this feature, but not its dominance. In addition, the large biases were likely related to the presence of water vapor, aerosols, and cloud contamination [13,35,36].

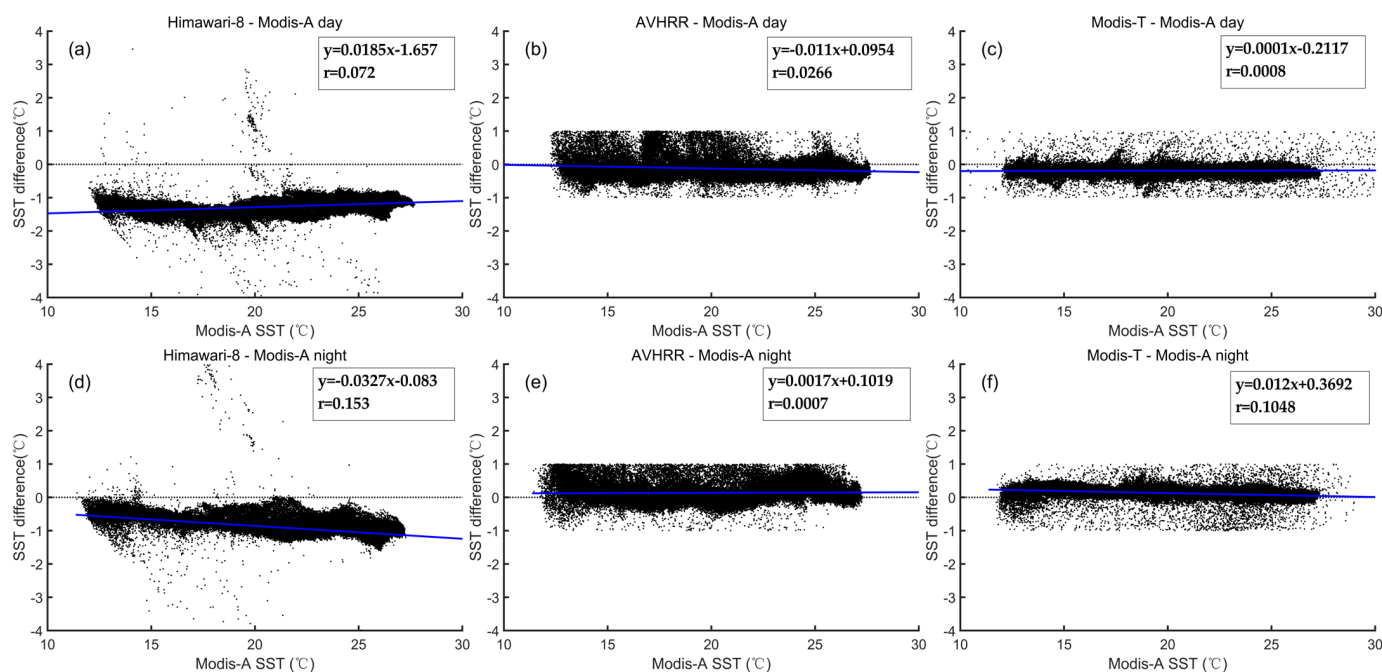


**Figure 7.** Scatter plots of the SST difference between three satellite with MODIS-Aqua as a function of MODIS-Aqua SST. (a): Himawari-8 daytime; (b): AVHRR daytime; (c): Modis-T daytime; (d): Himawari-8 nighttime; (e): AVHRR nighttime; (f): Modis-T nighttime. The blue solid line represents the fitted curve, and the dotted black line represents the 0 bias.

After analyzing the spatial distribution of the difference in sea surface temperature (SST) between the three satellites and MODIS-Aqua, the variations of this difference over time were also studied. Figure 8 illustrates the variations of the four satellites'

monthly SST from July 2015 to June 2021. Figures 9–11 depict the variations of monthly Bias, STD, and RMSE between the three satellites and MODIS-Aqua, respectively. The results indicate that Himawari-8's SST product consistently yielded lower values than MODIS-Aqua throughout the day (Figures 8 and 9), and the deviation between them had apparent seasonal variation (black line in Figure 9). Specifically, the monthly Bias of Himawari-8's daytime SST was highest in late winter and lowest in late summer (black line in Figure 9a), whereas the Bias of nighttime SST was highest in mid-winter (December) and lowest in mid-summer (July) (black line in Figure 9b). It is also noteworthy that although the Bias of daytime SST was larger than that of nighttime SST, the Bias fluctuation of nighttime was greater than that of daytime. The Bias of AVHRR was also mostly negative, with a smaller value than Himawari-8, but the variation was more complex than that of Himawari-8. In contrast to Himawari-8's daytime SST, the Bias of AVHRR's daytime SST was lowest in winter and highest in summer (blue line in Figure 9a). The Bias of AVHRR's nighttime SST was smaller than that of daytime SST, and there was no apparent seasonal variation (blue line in Figure 9b). Compared to Himawari-8 and AVHRR, the Bias of MODIS-Terra was the smallest and was positive during the day and negative at night (red line in Figure 9). Additionally, although the variation of MODIS-Terra Bias was relatively small, the value of Bias also exhibited the characteristic of being smaller in winter and larger in summer. It is worth noting that all three satellites had highly abnormal Bias values after December 2020. This coincidence indicates that the MODIS-Aqua-derived SST as a reference dataset may have outliers after December 2020.

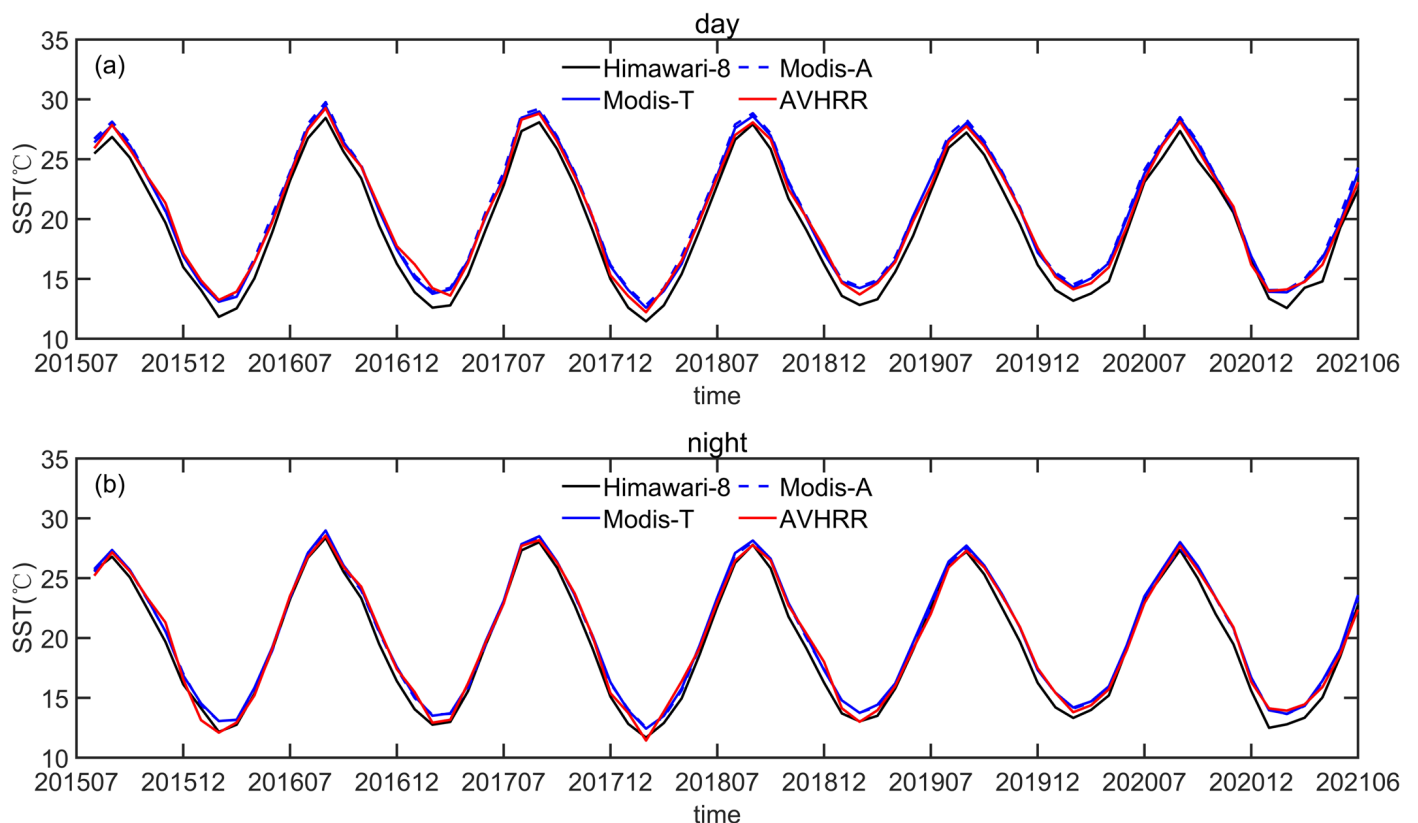


**Figure 8.** The time series of four satellite monthly SST from July 2015 to June 2021. (a) daytime; (b) nighttime.

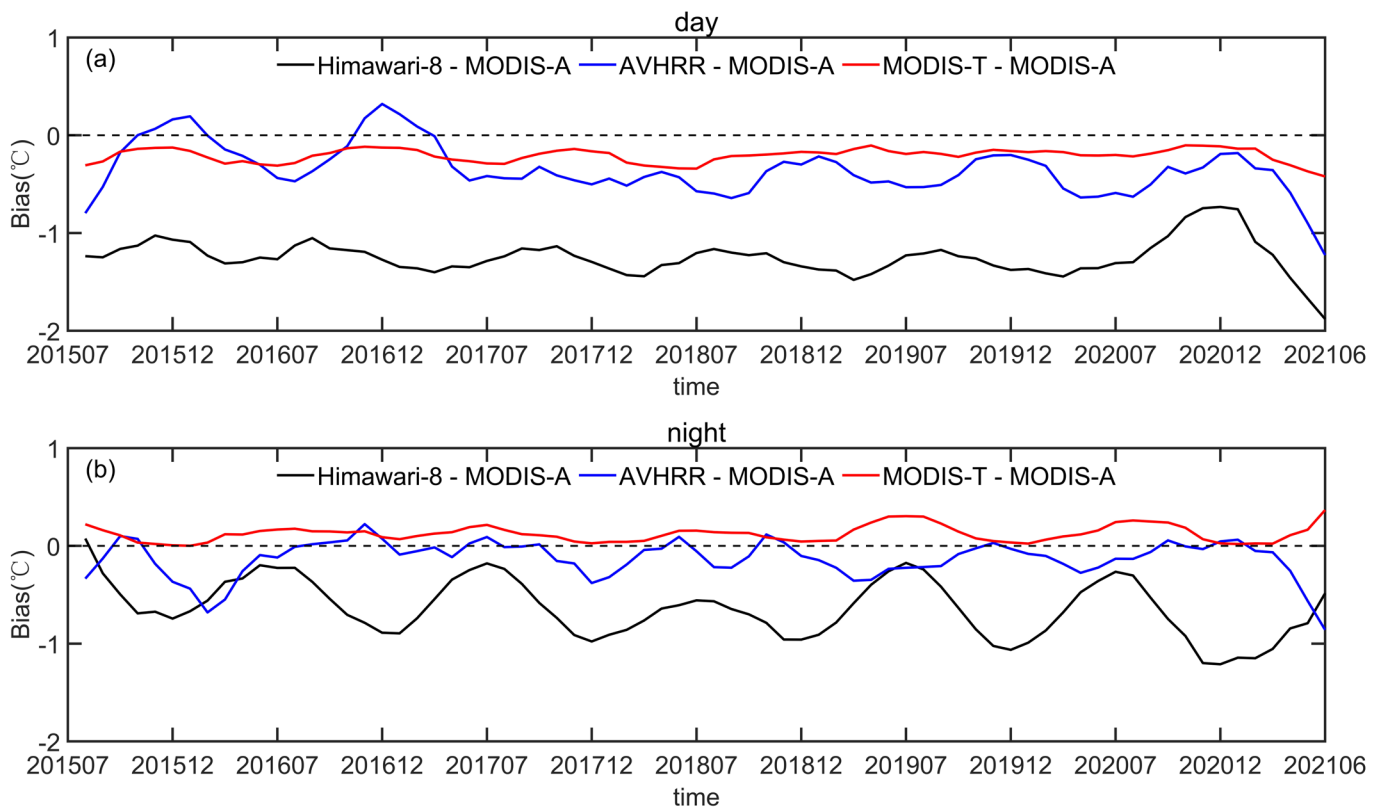


**Figure 9.** The time series of monthly Bias between three satellites and MODIS-Aqua from July 2015 to June 2021. (a) daytime; (b) nighttime.

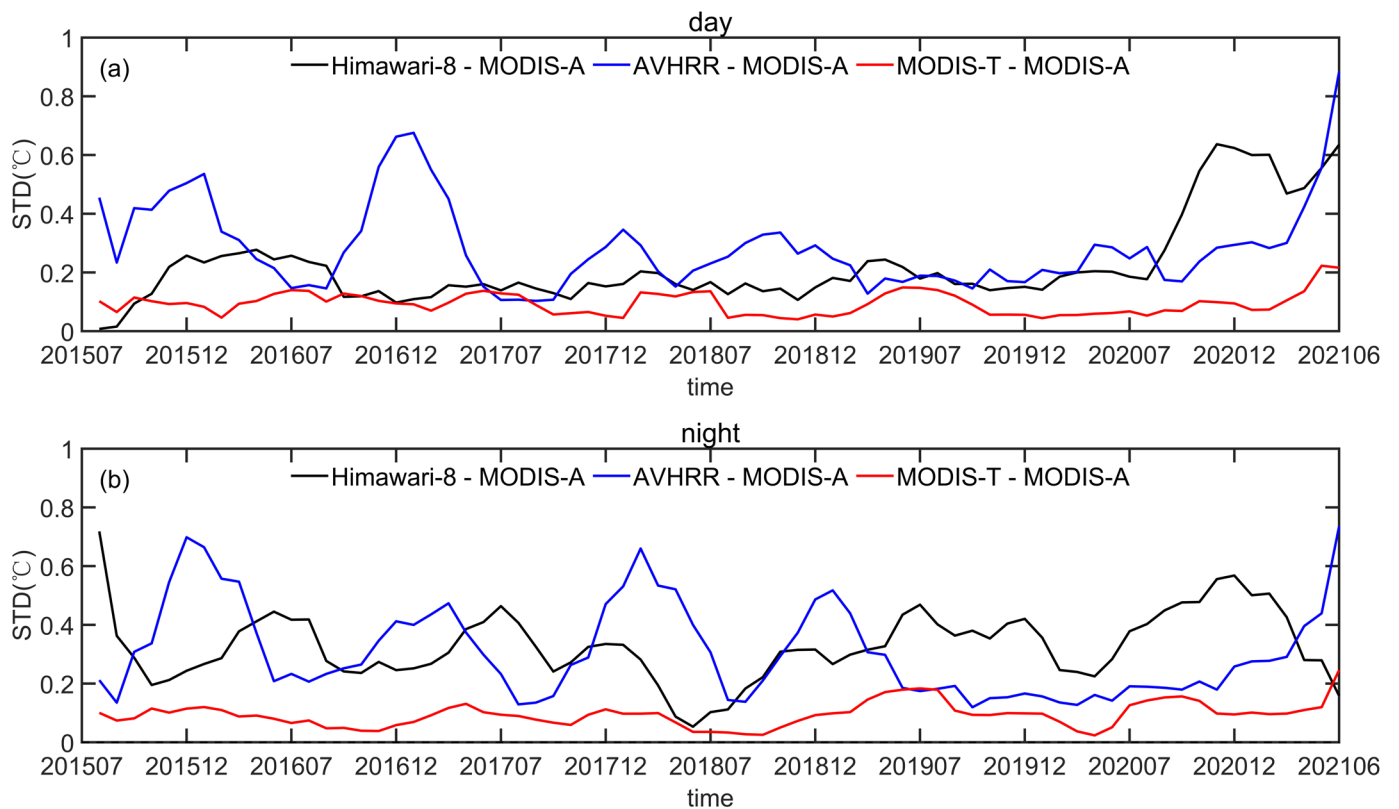


**Figure 10.** Time series of monthly STD between three satellites and MODIS-Aqua from July 2015 to June 2021. (a) daytime; (b) nighttime.

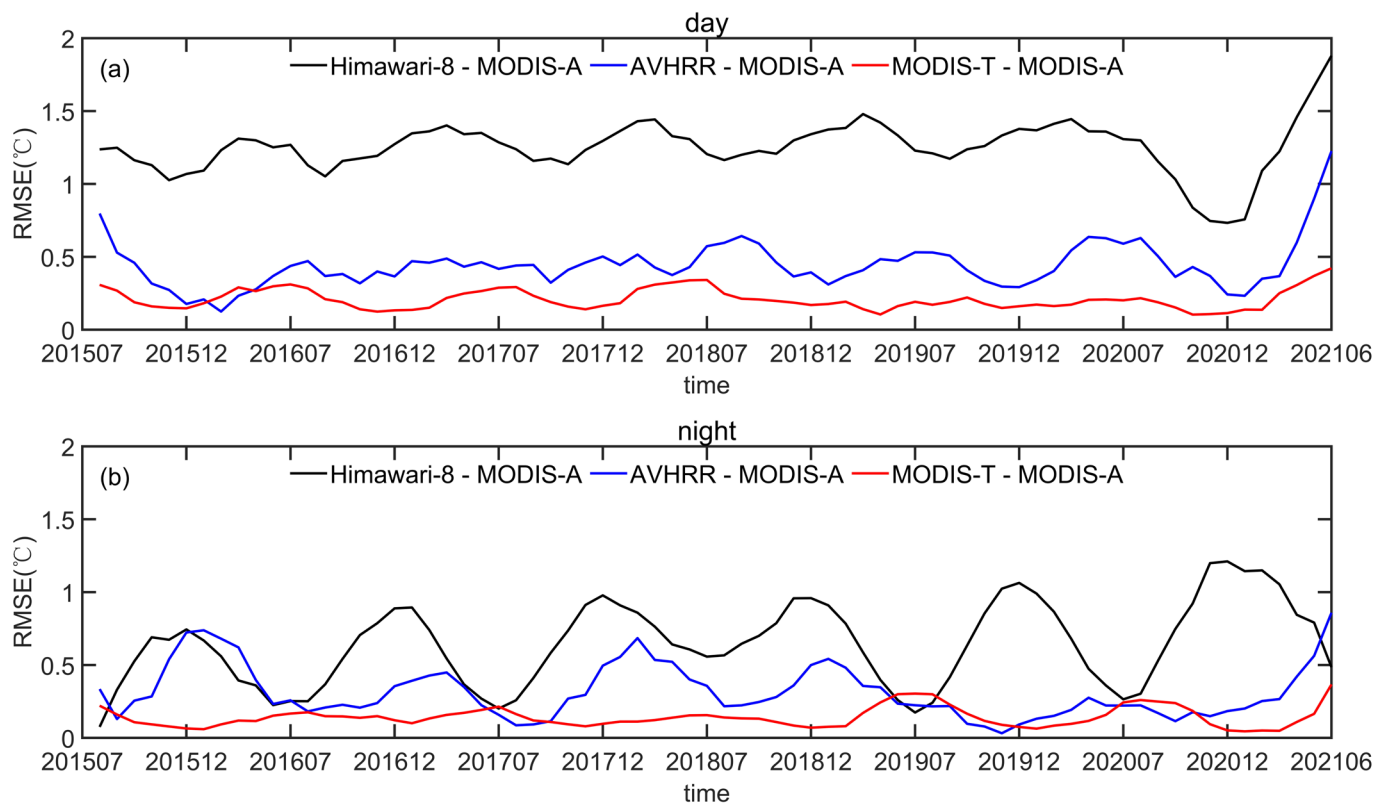


**Figure 11.** Time series of monthly RMSE between three satellites and MODIS-Aqua from July 2015 to June 2021. (a) daytime; (b) nighttime.

Standard deviation (STD) provides insight into the level of dispersion in the bias between two sets of satellite data, with a larger STD indicating greater fluctuation around the mean bias. Figure 10 displays the monthly STD between three satellites and MODIS-Aqua from July 2015 to June 2021. It can be seen that the daytime STD of Himawari-8 was relatively low before July 2020, with an average of roughly  $0.15\text{ }^{\circ}\text{C}$  (the black line in Figure 10a), while the nighttime STD was relatively high, with an average of about  $0.3\text{ }^{\circ}\text{C}$  (the black line in Figure 10b). The STD of AVHRR was relatively high both during the day and at night, with an average value of roughly  $0.3\text{ }^{\circ}\text{C}$  and a maximum value exceeding  $0.7\text{ }^{\circ}\text{C}$  (the blue line in Figure 10). The STD of MODIS-Terra was the smallest, with an average value of less than  $0.1\text{ }^{\circ}\text{C}$  (the red line in Figure 10).

Similar to the Bias, the Root Mean Square Error (RMSE) can also reflect the difference between two satellite datasets. However, since RMSE is the square root of the average of squared errors, it is always non-negative and can be used to compare the magnitude of positive and negative deviations. Figure 11 shows that the RMSE of daytime SST was generally higher than that of nighttime SST for the three satellites, but the oscillation of the RMSE showed the opposite trend, i.e., it was smaller in the daytime than at night, indicating that the deviation of daytime SST was larger and relatively stable, while the deviation of nighttime SST was small and had significant variations. The RMSE of Himawari-8 was larger in winter and smaller in summer. The RMSE of AVHRR nighttime SST showed the same variation; however, the RMSE of AVHRR daytime SST and MODIS-Terra showed opposite variations. It was also observed that in addition to the seasonal variation, the RMSE of Himawari-8 showed a long-term increasing trend.

#### 4. Discussion

The validation of the four satellite datasets using iQuam2 in situ measured SST data indicated that all four datasets demonstrated a good correlation ( $R > 0.99$ ) with the measured data and small errors, which is in line with previous research [11–14,16–18,24–26].

However, it should be noted that the measured data points were primarily distributed in offshore sea areas, with fewer data points in coastal regions, where water depths are shallower than 30 m (as shown in Figure 1). Due to the lack of in situ data in coastal sea areas, at present, it can only be proved that the error of MODIS-A was the smallest in the sea area deeper than 30 m. Therefore, the credibility of the error analysis results for nearshore areas with 30 m depth or less is uncertain. As such, the accuracy of satellite data in coastal regions with water depths less than 30 m needs to be evaluated more comprehensively by comparing it with additional measured data in the future.

Our research found a substantial discrepancy of approximately 0.2 °C in the bias of Himawari-8 as compared to the findings of prior studies [24,25]. The spatial distribution of errors, when compared with MODIS-Aqua as a reference dataset (depicted in Figures 6a and 7a), indicated that the errors in the Himawari-8 daytime SST data were proportionate to the latitude of the area. We speculate that the latitude-based variation of error was influenced by the variation of the zenith angle, which was higher at higher latitudes due to Himawari-8 being a geostationary satellite. Previous research on Himawari-8 has mainly focused on areas with lower latitudes, where the SST errors were minimal [24,37], and little attention has been paid to regions with higher latitudes. Tu et al. [25] conducted a study of the full disk area and concluded that the errors were smaller when the zenith angle was small; similarly, larger zenith angles resulted in greater errors. This is corroborated by other studies, which have also demonstrated the impact of different zenith angles on the accuracy of satellite SST observations [34,38]. As our study area is situated in the mid-latitude region, the higher zenith angle is likely to have a substantial impact on the accuracy of satellite SST monitoring, resulting in a larger error. Nevertheless, this is purely speculative, and further research is required to confirm whether the zenith angle is indeed a factor affecting the SST error.

Our accuracy validation results for AVHRR and MODIS were generally consistent with those of previous studies [11,12,16,17], though there may have been slight differences due to the varying study areas. However, the spatial distribution of errors for AVHRR exhibited different variation characteristics from previous studies, with larger errors observed in coastal regions (Figure 6b,e). These errors may have contributed significantly to the overall error. To investigate this issue, we analyzed the spatial coverage of AVHRR SST data in the coastal region for each month. For instance, the spatial coverage of AVHRR SST data in the four seasons of 2016 was examined (Figure 12), revealing poor spatial coverage in the coastal area, particularly during winter. Thus, when we used the regional average of SST for cross-comparison with measured data, the absence of coastal data may have resulted in large errors in the calculated regional average. This absence of AVHRR coastal data is due to the fact that AVHRR SST is reprocessed data and strictly excludes data from areas with more cloud coverage [18], which has a significant impact on the spatial coverage of data in coastal regions [39]. Furthermore, the large errors of AVHRR in coastal areas may have also been associated with the AVHRR SST monthly data synthesis algorithm.

In terms of temporal variation, the errors exhibited by all four datasets demonstrated seasonal variation characteristics, with Bias and RMSE varying considerably. These observations are consistent with previous studies [18,40]. However, the underlying causes of this seasonal variation are not well understood. To elucidate possible causes, we plotted the month-by-month evolution of satellite coverage for the six-year period spanning from July 2015 to June 2021 (Figure 13). Remarkably, we found that the coverage of all four datasets was closely aligned with the seasonal variation of the error, exhibiting a low during winter and a high during summer. Thus, we posit that the seasonal variation of satellite data errors may be influenced by the seasonal variation of data spatial coverage. Low spatial coverage tends to result in higher data error, whereas high spatial coverage corresponds with lower data error. We further noted that AVHRR exhibited a significant variation in error during the daytime between July 2015 and June 2017 (Figures 9a, 10a and 11a). Analysis of the corresponding spatial coverage curve (Figure 13) revealed that the fluctuation in AVHRR's spatial coverage was also considerable during this period. This finding corroborates the

hypothesis that poor spatial coverage of AVHRR may lead to low data quality and increased data uncertainty.

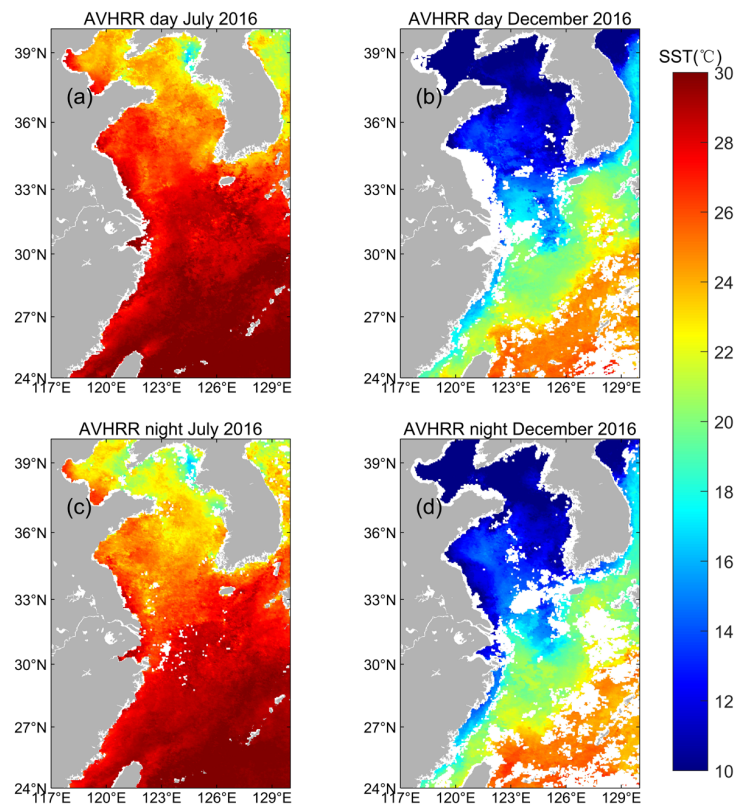


**Figure 12.** Spatial distribution of AVHRR SST in summer and winter in 2016. The monthly daytime SST for July (a) and December (b); The monthly nighttime SST for July (c) and December (d).

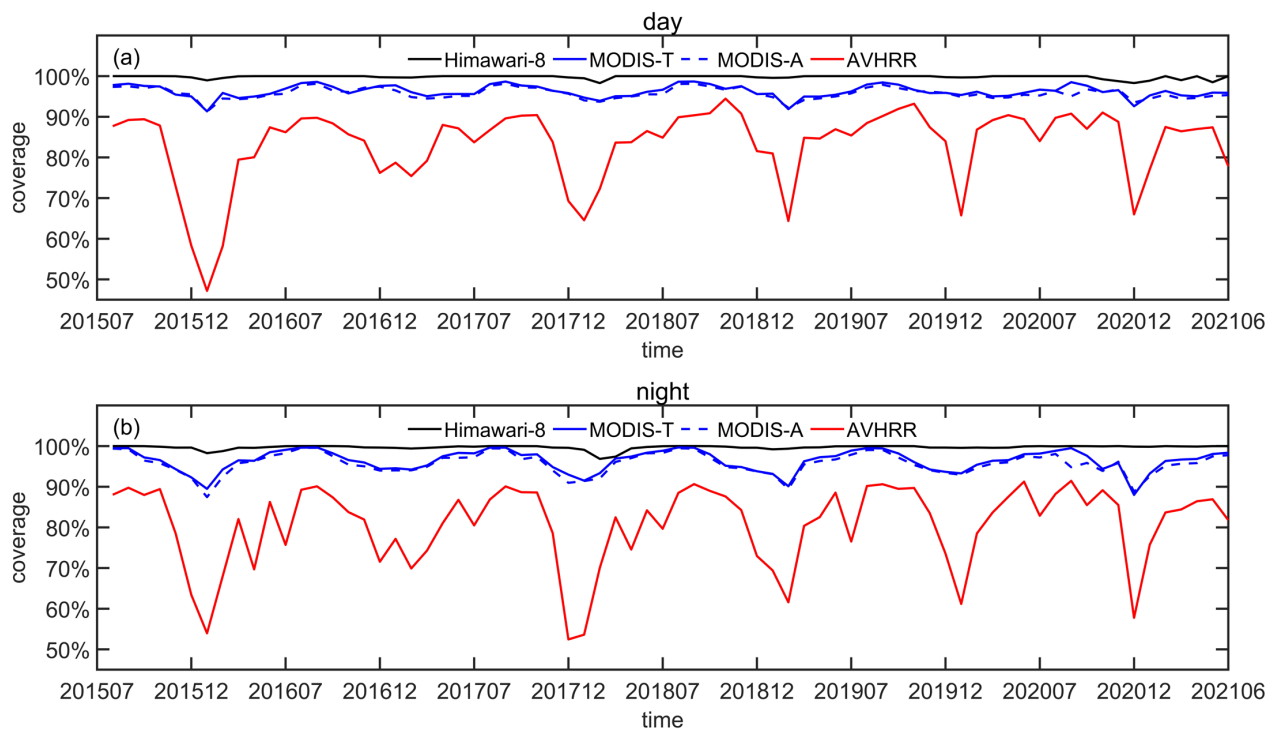


**Figure 13.** Monthly variation of the four satellite data SST coverage from July 2015 to June 2021. (a) daytime; (b) nighttime.

Furthermore, we observed from the statistical graphs depicting the error of the three datasets compared to Modis-A (Figures 9–11) that while the error exhibited more significant fluctuations at night compared to during the day, the error magnitude itself was relatively lower and more consistent at night. Considering the complexity of the inversion algorithm and the impact of cloud coverage, it is possible that the quality of the data during nighttime may be superior to that of the daytime. Consequently, some scholars have exclusively employed nighttime data for comparisons and analyses [34]. However, a deeper investigation into whether nighttime data are genuinely superior to daytime data, and the underlying reasons for such findings, is required in the future and will not be expounded upon here.

It is worth noting that the error curves for all three datasets in comparison to Modis-A (shown in Figures 9–11) displayed a significant shift after December 2020. Given that this paper utilized Modis-A as the benchmark dataset, it is possible that Modis-A exhibited a greater error during this time period. Hence, the analysis of Modis-A's error in this study may be incomplete, and further investigation into Modis-A's error is necessary.

## 5. Conclusions

This paper aimed to validate the accuracy of sea surface temperature products obtained from four satellite data sources, namely Himawari-8, AVHRR, Modis-Terra, and Modis-Aqua, in the Bohai-Yellow-East China Sea (BYECS). To achieve this goal, we analyzed the errors using iQuam2 in situ SST. After that, we selected the Modis-A data with the smallest error as the validation dataset for the last six years (July 2015–June 2021) of the other three satellite data sources. We conducted a comparative analysis of these datasets to evaluate the SST data characteristics of both polar and geostationary satellites. This included spatial and temporal comparisons. Finally, we analyzed the characteristics of space and time distribution and the proposed possible reasons for such characteristics.

The results revealed a strong correlation between satellite and in situ data, with R correlation coefficients exceeding 0.99. However, the analysis uncovered variations in the precision of the satellite datasets, with Himawari-8 exhibiting the greatest deviation error, and MODIS-Aqua displaying the smallest error. The biases, RMSE, and STD results further supported these conclusions. While annual errors were generally insignificant, some collocated points exhibited substantial hourly errors. Himawari-8 demonstrated the highest hourly error, with maximum values of bias and RMSE reaching up to 6 °C from in situ measured data. Moreover, Himawari-8 also exhibited the highest error fluctuation, while the other three satellites had lesser fluctuations. Positive/negative hourly bias indicated that the errors in Himawari-8 and AVHRR SST data were greater when underestimated, whereas the opposite was true for the two MODIS satellites.

A spatial analysis of the satellite-derived SST difference between three satellites and MODIS-Aqua over a period of six years revealed variations in the average SST values. The Himawari-8 SST data exhibited lower values in the BYECS region, with greater deviation during the day compared to the nighttime, while the AVHRR SST data were higher than those of MODIS-Aqua in the nearshore region. Additionally, the SST data from AVHRR and Himawari-8 had a lower/higher deviation during the daytime/nighttime than MODIS-Aqua in certain areas. Conversely, the SST values from MODIS-Terra were only slightly different from those in the MODIS-Aqua. Our analysis of SST deviation between three satellites and MODIS-Aqua at different water temperatures showed that the deviation was influenced by both the satellite and water temperature. The SST deviation between Himawari-8 and MODIS-Aqua was predominantly negative and decreased with increasing water temperature during the day. However, the retrieval error at night increased as the water temperature rose. The deviation of MODIS-Terra was the smallest and decreased with increasing water temperature. The temporal variations of SST differences between three satellites and MODIS-Aqua showed that the SST from Himawari-8 was consistently lower than that of MODIS-Aqua, with apparent seasonal variation. The bias of AVHRR was also negative, with a more complex variation than that of Himawari-8. Compared to Himawari-8 and AVHRR, the bias of MODIS-Terra was the smallest and exhibited positive

values during the day and negative values at night. All three satellites showed highly abnormal bias values after December 2020, indicating that the MODIS-Aqua-derived SST as a reference dataset may have outliers after this time. Compared with MODIS-Aqua, the standard deviation (STD) of Himawari-8 was relatively low during the day and high at night, while the STD of AVHRR was relatively high both during the day and at night. The root mean square error (RMSE) of daytime SST was generally higher than that of nighttime SST for the three satellites, and the oscillation of the RMSE was the opposite between daytime and nighttime. Additionally, the RMSE of Himawari-8 showed a long-term increasing trend.

The four distinct types of satellite data each possess their own merits and drawbacks. Himawari-8 offers remarkable temporal and spatial resolution, as well as expansive spatial coverage, yet suffers from significant inaccuracies. Conversely, the other three satellite data types exhibit inferior resolution and coverage when compared to Himawari-8 but are characterized by smaller errors. In circumstances involving the short-term analysis of areas under geostationary satellite coverage, we observed that geostationary satellites are better suited than pole-orbiting satellites, particularly in areas featuring relatively low latitudes, where their accuracy is comparatively high. Conversely, for areas outside of geostationary satellite coverage or for long-term investigations, polar orbiting satellites are better suited. MODIS data, in particular, offer relatively greater accuracy. Moving forward, the various spatial and temporal attributes of the four types of satellite data can be expertly utilized and combined with relevant fusion algorithms to create highly precise, expansive, and detailed sea surface temperature products. This would provide a valuable data foundation for subsequent analyses and research. Additional data processing of AVHRR is also required, including interpolation of missing data and adjustment of the monthly data synthesis algorithm.

**Author Contributions:** Conceptualization, W.Y. and S.H.; methodology, C.F., W.Y. and S.H.; software, C.F.; validation, W.Y. and S.H.; formal analysis, M.H. and X.L.; data curation, C.F. and W.Y.; writing—original draft preparation, C.F. and W.Y.; writing—review and editing, W.Y., S.H. and X.L.; visualization, C.F.; supervision, W.Y. and S.H.; funding acquisition, W.Y. and S.H. All authors have read and agreed to the published version of the manuscript.

**Funding:** This research was funded by the National Natural Science Foundation of China, grant number (41906025), the Hainan Provincial Natural Science Foundation of China, grant number (420QN289), the National Natural Science Foundation of China, grant number (41876031).

**Data Availability Statement:** The JAXA-SST data used in this study can be downloaded from the Japan Aerospace Exploration Agency (<http://www.eorc.jaxa.jp/ptree> accessed on 12 June 2022); the AVHRR SST data used in this study can be downloaded from NOAA National Centers for Environmental Information (<https://www.ncei.noaa.gov/products/avhrr-pathfinder-sst/> accessed on 21 June 2022); the MODIS SST data used in this study can be downloaded from NASA OceanColor SST System (<https://oceandata.sci.gsfc.nasa.gov/directdataaccess/> accessed on 6 June 2022); the iQuam in situ SST data used in this paper can be downloaded from NOAA Center for in situ SST Quality Monitor (<https://www.star.nesdis.noaa.gov/socd/sst/iquam/> accessed on 5 June 2022).

**Conflicts of Interest:** The authors declare no conflict of interest.

## References

1. Yang, Y.-C.; Lu, C.-Y.; Huang, S.-J.; Yang, T.-Z.; Chang, Y.-C.; Ho, C.-R. On the Reconstruction of Missing Sea Surface Temperature Data from Himawari-8 in Adjacent Waters of Taiwan Using DINEOF Conducted with 25-h Data. *Remote Sens.* **2022**, *14*, 2818. [[CrossRef](#)]
2. Bao, X.; Wan, X.; Gao, G.; Wu, D. The characteristics of the seasonal variability of the sea surface temperature field in the Bohai Sea, the Huanghai Sea and the East China Sea from AVHRR data. *Acta Oceanol. Sin.* **2002**, *24*, 125–133.
3. García-Monteiro, S.; Sobrino, J.A.; Julien, Y.; Sòria, G.; Skokovic, D. Surface Temperature trends in the Mediterranean Sea from MODIS data during years 2003–2019. *Reg. Stud. Mar. Sci.* **2022**, *49*, 102086. [[CrossRef](#)]
4. Mohamed, B.; Nilsen, F.; Skogseth, R. Interannual and Decadal Variability of Sea Surface Temperature and Sea Ice Concentration in the Barents Sea. *Remote Sens.* **2022**, *14*, 4413. [[CrossRef](#)]

5. Tang, X.; Wang, F.; Chen, Y.; Li, M. Warming trend in northern East China Sea in recent four decades. *Chin. J. Oceanol. Limnol.* **2009**, *27*, 185–191. [[CrossRef](#)]
6. Zhang, L.; Wu, L.; Lin, X.; Wu, D. Modes and mechanisms of sea surface temperature low-frequency variations over the coastal China seas. *J. Geophys. Res.* **2010**, *115*, C08031. [[CrossRef](#)]
7. Zhang, H.; Ignatov, A. A Completeness and Complementarity Analysis of the Data Sources in the NOAA In Situ Sea Surface Temperature Quality Monitor (iQuam) System. *Remote Sens.* **2021**, *13*, 3741. [[CrossRef](#)]
8. Alerksans, E.; Høyer, J.L.; Gentemann, C.L.; Pedersen, L.T.; Nielsen-Englyst, P.; Donlon, C. Construction of a climate data record of sea surface temperature from passive microwave measurements. *Remote Sens. Environ.* **2020**, *236*, 111485. [[CrossRef](#)]
9. Cao, M.; Mao, K.; Yan, Y.; Shi, J.; Wang, H.; Xu, T.; Fang, S.; Yuan, Z. A new global gridded sea surface temperature data product based on multisource data. *Earth Syst. Sci. Data* **2021**, *13*, 2111–2134. [[CrossRef](#)]
10. Koutantou, K.; Brunner, P.; Vazquez-Cuervo, J. Validation of NASA Sea Surface Temperature Satellite Products Using Saildrone Data. *Remote Sens.* **2023**, *15*, 2277. [[CrossRef](#)]
11. Gong, S.; Wong, K. Spatio-temporal analysis of sea surface temperature in the East China Sea using TERRA/MODIS products data. *Sea Level Rise Coast. Infrastruct.* **2018**, *13*, 213–227.
12. Hao, Y.; Cui, T.; Singh, V.P.; Zhang, J.; Yu, R.; Zhang, Z. Validation of MODIS Sea Surface Temperature Product in the Coastal Waters of the Yellow Sea. *IEEE J. Sel. Top. Appl. Earth Obs. Remote Sens.* **2017**, *10*, 1667–1680. [[CrossRef](#)]
13. Saleh, A.K.; Al-Anzi, B.S. Statistical Validation of MODIS-Based Sea Surface Temperature in Shallow Semi-Enclosed Marginal Sea: A Comparison between Direct Matchup and Triple Collocation. *Water* **2021**, *13*, 1078. [[CrossRef](#)]
14. Kozlov, I.; Dailidienė, I.; Korosov, A.; Klemas, V.; Mingėlaitė, T. MODIS-based sea surface temperature of the Baltic Sea Curonian Lagoon. *J. Mar. Syst.* **2014**, *129*, 157–165. [[CrossRef](#)]
15. Shuva, M.S.H.; Golder, M.R.; Rouf, M.A.; Uddin, M.M.; Bir, J. Daytime and nighttime sea surface temperature (SST) along with diurnal variability (D-SST) in the northern bay of bengal: A remote sensing approach. *Thalass. Int. J. Mar. Sci.* **2022**, *38*, 697–708. [[CrossRef](#)]
16. Chen, Y.; Qu, L.; Guan, L. Evaluation of NOAA/AVHRR Sea Surface Temperature at Full HRPT Resolution in the Northwest Pacific Ocean. *J. Ocean Univ. China* **2021**, *20*, 1431–1439. [[CrossRef](#)]
17. Qiu, C.; Wang, D.; Kawamura, H.; Guan, L.; Qin, H. Validation of AVHRR and TMI-derived sea surface temperature in the northern South China Sea. *Cont. Shelf Res.* **2009**, *29*, 2358–2366. [[CrossRef](#)]
18. Meng, X.; Qingtao, S.; Mingsen, L. Comparison in multi-infrared products of sea surface temperature in northwest pacific. *Oceanol. Limnol. Sin* **2017**, *48*, 436–453.
19. Yin, W.; Ma, Y.; Wang, D.; He, S.; Huang, D. Surface Upwelling off the Zhoushan Islands, East China Sea, from Himawari-8 AHI Data. *Remote Sens.* **2022**, *14*, 3261. [[CrossRef](#)]
20. Xie, S.; Huang, Z.; Wang, X.H.; Lepastrier, A. Quantitative Mapping of the East Australian Current Encroachment Using Time Series Himawari-8 Sea Surface Temperature Data. *J. Geophys. Res. Ocean.* **2020**, *125*, e2019JC015647. [[CrossRef](#)]
21. Hu, Z.; Xie, G.; Zhao, J.; Lei, Y.; Xie, J.; Pang, W. Mapping Diurnal Variability of the Wintertime Pearl River Plume Front from Himawari-8 Geostationary Satellite Observations. *Water* **2021**, *14*, 43. [[CrossRef](#)]
22. Huang, C.; Liu, Y.; Luo, Y.; Wang, Y.; Liu, X.; Zhang, Y.; Zhuang, Y.; Tian, Y. Improvement and Assessment of Ocean Color Algorithms in the Northwest Pacific Fishing Ground Using Himawari-8, MODIS-Aqua, and VIIRS-SNPP. *Remote Sens.* **2022**, *14*, 3610. [[CrossRef](#)]
23. Huang, Z.; Feng, M.; Beggs, H.; Wijffels, S.; Cahill, M.; Griffin, C. High-resolution marine heatwave mapping in Australasian waters using Himawari-8 SST and SSTAARS data. *Remote Sens. Environ.* **2021**, *267*, 112742. [[CrossRef](#)]
24. Ditri, A.; Minnett, P.; Liu, Y.; Kilpatrick, K.; Kumar, A. The Accuracies of Himawari-8 and MTSAT-2 Sea-Surface Temperatures in the Tropical Western Pacific Ocean. *Remote Sens.* **2018**, *10*, 212. [[CrossRef](#)]
25. Tu, Q.G.; Hao, Z.Z. Validation of Sea Surface Temperature Derived From Himawari-8 by JAXA. *IEEE J. Sel. Top. Appl. Earth Obs. Remote Sens.* **2020**, *13*, 448–459. [[CrossRef](#)]
26. Kurihara, Y.; Murakami, H.; Kachi, M. Sea surface temperature from the new Japanese geostationary meteorological Himawari-8 satellite. *Geophys. Res. Lett.* **2016**, *43*, 1234–1240. [[CrossRef](#)]
27. Saha, K.; Zhao, X.; Zhang, H.-M.; Casey, K.; Zhang, D.; Baker-Yeboah, S.; Kilpatrick, K.; Evans, R.; Ryan, T.; Relph, J. *AVHRR Pathfinder Version 5.3 Level 3 Collated (L3C) Global 4km Sea Surface Temperature for 1981-Present*; NOAA National Centers for Environmental Information: Asheville, NC, USA, 2018.
28. Kilpatrick, K.; Podesta, G.; Evans, R. Overview of the NOAA/NASA advanced very high resolution radiometer Pathfinder algorithm for sea surface temperature and associated matchup database. *J. Geophys. Res. Ocean.* **2001**, *106*, 9179–9197. [[CrossRef](#)]
29. Saha, K.; Dash, P.; Zhao, X.; Zhang, H.-m. Error estimation of pathfinder version 5.3 level-3C SST using extended triple collocation analysis. *Remote Sens.* **2020**, *12*, 590. [[CrossRef](#)]
30. Esaias, W.E.; Abbott, M.R.; Barton, I.; Brown, O.B.; Campbell, J.W.; Carder, K.L.; Clark, D.K.; Evans, R.H.; Hoge, F.E.; Gordon, H.R. An overview of MODIS capabilities for ocean science observations. *IEEE Trans. Geosci. Remote Sens.* **1998**, *36*, 1250–1265. [[CrossRef](#)]
31. Xu, F.; Ignatov, A. In situ SST Quality Monitor (iQuam). *J. Atmos. Ocean. Technol.* **2014**, *31*, 164–180. [[CrossRef](#)]
32. Xu, F.; Ignatov, A. Error characterization in iQuam SSTs using triple collocations with satellite measurements. *Geophys. Res. Lett.* **2016**, *43*, 10826–10834. [[CrossRef](#)]

33. Wang, H.; Lin, M.; Ma, C.; Yin, X.; Guan, L. Evaluation of Sea Surface Temperature from HY-1C Data. In Proceedings of the IGARSS 2020–2020 IEEE International Geoscience and Remote Sensing Symposium, Waikoloa, HI, USA, 26 September–2 October 2020; pp. 5897–5900.
34. López García, M.J. SST Comparison of AVHRR and MODIS Time Series in the Western Mediterranean Sea. *Remote Sens.* **2020**, *12*, 2241. [[CrossRef](#)]
35. Zhu, Y.; Bo, Y.; Zhang, J.; Wang, Y. Fusion of Multisensor SSTs Based on the Spatiotemporal Hierarchical Bayesian Model. *J. Atmos. Ocean. Technol.* **2018**, *35*, 91–109. [[CrossRef](#)]
36. Dong, S.; Gille, S.T.; Sprintall, J.; Gentemann, C. Validation of the Advanced Microwave Scanning Radiometer for the Earth Observing System (AMSR-E) sea surface temperature in the Southern Ocean. *J. Geophys. Res.* **2006**, *111*, C04002. [[CrossRef](#)]
37. Sukresno, B.; Hanintyo, R.; Kusuma, D.W.; Jatisworo, D.; Murdimanto, A. Three-Way Error Analysis of Sea Surface Temperature (Sst) Between Himawari-8, Buoy, and Mur Sst in Savu Sea. *Int. J. Remote Sens. Earth Sci.* **2018**, *15*, 25–36. [[CrossRef](#)]
38. Park, K.-A.; Woo, H.-J.; Chung, S.-R.; Cheong, S.-H. Development of Sea Surface Temperature Retrieval Algorithms for Geostationary Satellite Data (Himawari-8/AHI). *Asia Pac. J. Atmos. Sci.* **2019**, *56*, 187–206. [[CrossRef](#)]
39. Bulgin, C.E.; Embury, O.; Merchant, C.J. Sampling uncertainty in gridded sea surface temperature products and Advanced Very High Resolution Radiometer (AVHRR) Global Area Coverage (GAC) data. *Remote Sens. Environ.* **2016**, *177*, 287–294. [[CrossRef](#)]
40. Xu, Y.; Li, L.; Xue, C.; Yue, Z.; Liu, J. Sea surface temperature consistency analysis based on AVHRR and MODIS. *Mar. Environ. Sci.* **2021**, *40*, 122–132. [[CrossRef](#)]

**Disclaimer/Publisher’s Note:** The statements, opinions and data contained in all publications are solely those of the individual author(s) and contributor(s) and not of MDPI and/or the editor(s). MDPI and/or the editor(s) disclaim responsibility for any injury to people or property resulting from any ideas, methods, instructions or products referred to in the content.